Controllable magnetic states in chains of coupled φ_0 Josephson junctions with ferromagnetic weak links

G. A. Bobkov,[1] I. V. Bobkova,[1,2] and A. M. Bobkov[1]
[1]*Moscow Institute of Physics and Technology, Dolgoprudny 141700, Russia*
[2]*Higher School of Economics, National Research University, Moscow 101000, Russia*

(Received 25 October 2023; revised 9 February 2024; accepted 12 February 2024; published 27 February 2024)

A superconductor/ferromagnet/superconductor Josephson junction with anomalous phase shift (φ_0-S/F/S JJ) is a system in which the anomalous ground state shift φ_0 provides direct magnetoelectric coupling between a magnetic moment and a phase of the superconducting condensate. If a chain of such φ_0-S/F/S JJs are coupled via superconducting leads, the condensate phase, being a macroscopic quantity, mediates a long-range interaction between the magnetic moments $\boldsymbol{M}_i$ of the weak links. We study the static and dynamic magnetic properties of such a system. It is shown that it manifests properties of an n-level system, in which the energies of the levels are determined by only projections of the total magnetic moment $\sum \boldsymbol{M}_i$ onto the easy magnetic axis. It is similar to a magnetic atom in a Zeeman field, but the role of the field is played by the magnetoelectric coupling. However, unlike an atom in a magnetic field, the relative order of energies of different states is controlled by electrical means. It is also demonstrated that $\sum \boldsymbol{M}_i$ can be fully controlled by a supercurrent and the response of the magnetic system to local external perturbations is highly nonlocal.

DOI: 10.1103/PhysRevB.109.054523

I. INTRODUCTION

The physics of equilibrium magnetic states and magnetic excitations crucially depends on the type of magnetic interaction between the magnetic moments. Direct and indirect exchange interactions, spin-orbit effects, and dipole-dipole interactions lead to a large number of different magnetic states, including ferromagnetism, antiferromagnetism, altermagnetism, helimagnetism, skyrmions, spin glasses, etc. Another interesting direction is the interaction of more macroscopic magnets, which is very important, for example, for magnetoresistive phenomena [1,2]. It can be realized via indirect interlayer exchange interaction [3–5], via dipole-dipole interaction, and, more relevant to the subject of the present paper, via superconductors.

Coupling via superconductors can be realized by different physical mechanisms. One of them is the proximity effect. As first pointed out by de Gennes, a superconductor makes the antiferromagnetic configuration of magnets more favorable [6]. The reason is that with such a mutual orientation of magnets, superconductivity in the interlayer is less suppressed as a result of partial compensation of paramagnetic depairing. The characteristic scale of such an interaction is the superconducting coherence length ξ_S. A lot of theoretical proposals and experimental realizations of a superconducting spin valve have been based on the interaction via the proximity effect [7–14]. Later, it was proposed [15] that the interaction between magnets can also be mediated by the electromagnetic proximity effect [16], the essence of which is the appearance of Meissner currents in a superconductor in response to the presence of an adjacent magnetic material. The characteristic scale of this coupling is the penetration depth of the magnetic field λ.

Recently, another mechanism for establishing interaction between magnetic moments was proposed. It is not related to the proximity effects and is based on another physical principle. The interaction is of magnetoelectric origin and is mediated by supercurrents, which makes it extremely long range and decay according to a power law. The magnetoelectric coupling was considered both for magnetic impurities in superconductors [17–19] and for weak links of coupled Josephson junctions (JJs) [20]. In the last case the interaction is mediated by the phase of a superconducting condensate, which is a macroscopic quantity. For this reason the characteristic scale of the interaction is not restricted by the typical proximity scales of a superconductor, such as ξ_S and λ, and can be much larger [20].

The coupling between the superconducting phase and the magnetic moment is realized in JJs with a strong spin-orbit coupling in the interlayer region [21–32] or in JJs on a topological insulator [33–37], where the surface conduction electrons have the property of full spin-momentum locking [38–41]. Physically, the presence of the coupling between the superconducting phase and the magnetic moment in JJs manifests in the form of the so-called anomalous phase shift in the ground state of the junction [42,43]. The essence of this effect is that under the simultaneous breaking of inversion symmetry, which allows for the spin-orbit coupling (SOC), and time-reversal symmetry, which is due to the presence of the magnetic moment, a supercurrent can be induced in the JJ at zero phase difference between the leads. In the ground state of the junction this "anomalous supercurrent" is compensated by the phase shift $\varphi_0 \neq 0, \pi$, which is called the anomalous ground state phase shift, and the JJs manifesting this effect are called φ_0-JJs.

The breaking of the time-reversal symmetry can be achieved more easily by applying a magnetic field to the JJ. JJs with anomalous phase shift generated by the Zeeman effect of the applied magnetic field have already been implemented experimentally by several groups [44–47], including on a topological insulator. Realization of φ_0-superconductor/ferromagnet/superconductor JJs (φ_0-S/F/S JJs) is a more challenging problem, but the possibility to obtain in such systems direct coupling between the magnetization of the weak link and the superconducting phase opens great prospects for applications of such structures for controlling magnetization [42,48–53]. One of the possibilities is to use two-dimensional (2D) or quasi-2D ferromagnets, in which the Rashba spin-orbit coupling can be strong due to the structural inversion symmetry breaking, for the interlayers. The other way is to exploit ferromagnetic insulator/three-dimensional topological insulator (3D TI) hybrids as interlayers [54–61].

Reference [20] showed that in a system of two coupled φ_0-JJs with ferromagnetic weak links characterized by magnetic moments $\boldsymbol{M}_{1,2}$ the magnetic state of the system, that is, the directions of both magnetizations, can be fully controlled by the phase difference between the external superconducting leads. It was found that at large values of the phase difference the most favorable state of the magnets is ferromagnetic, and the directions of both magnetizations are dictated by the phase. At the same time, at small values of the phase difference the most favorable state is antiferromagnetic. In this case the state of a given magnet is not fixed by the phase, and therefore, there is an indirect interaction between them which is mediated by the superconducting phase.

In the present paper we continue investigations of coupled φ_0-S/F/S JJs and generalize the results of Ref. [20] to the case with an arbitrary number of coupled JJs. We find that the system with an arbitrary number of easy-axis magnets, which are weak links of the φ_0-JJs, behaves like a magnetic atom in some aspects. States with different projections of the total magnetic moment $\sum \boldsymbol{M}_i$ onto the easy axis (where the sum is taken over all the weak links) are degenerate in the absence of interaction mediated by the condensate phase, i.e., above the critical temperature of the superconductor or in the absence of the anomalous phase shift. Including the interaction removes this degeneracy, similar to the case of a magnetic atom in a Zeeman field. However, unlike an atom in a magnetic field, the relative energies of different projections of the total magnetic moment are controlled by the external phase difference.

This paper is organized as follows. In Sec. II we describe the system and the model which we study. Section III is devoted to an investigation of the equilibrium magnetic state of the system. In Sec. IV we study the dynamical processes of the transition of the system between different stable states. In Sec. V we discuss the influence of the possible nonequivalence of different JJs on the effects considered above. Our conclusions are presented in Sec. VI.

II. MODEL

We consider a linear chain of N coupled φ_0-S/F/S JJs, where S indicates a conventional superconductor and F stands for a homogeneous ferromagnet with magnetic moment $\boldsymbol{M}_i$,

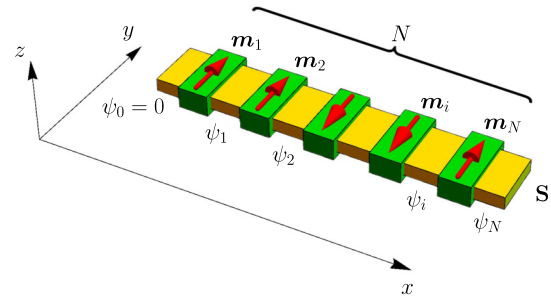

FIG. 1. Sketch of a coupled system of N φ_0-S/F/S JJs. The magnetic moment of each JJ is shown by a red arrow. ψ_i is a phase of the superconducting region connecting the ith and $(i+1)$th weak links with respect to the phase of the left lead, which is taken to be zero.

where i is the number of the weak link in the chain. Further, we introduce unit vectors along the direction of the corresponding magnetization $\boldsymbol{m}_i = \boldsymbol{M}_i/|\boldsymbol{M}_i|$. It is assumed that the ferromagnets are easy-axis magnets with the easy axis along the y direction. A sketch of the system is shown in Fig. 1. The superconducting phase difference ψ_N between the leads is an external controlling parameter.

The physical origin of the inversion symmetry breaking leading to the φ_0 behavior can be different and does not influence our conclusions. For example, for the interlayers, one can use a few monolayer van der Waals ferromagnets up to the monolayer limit [62–64], where the Rashba SOC can be intrinsic or due to the structural inversion symmetry breaking. The other possibility is a complex interlayer made of a combination of a thin-film ferromagnet and a heavy metal layer like Pt, providing strong SOC. The interlayer can also be composed of a ferromagnetic insulator on top of the 3D TI, as mentioned in the Introduction. If the ferromagnet is an insulator, it is assumed that the magnetization $\boldsymbol{M}$ of the ferromagnet induces an effective exchange field $\boldsymbol{h} \sim \boldsymbol{M}$ in the underlying conductive layer.

The current-phase relation of each of the φ_0-S/F/S JJs in the chain takes the form $I = I_{c,i}\sin(\chi_i - \varphi_{0,i})$, where $I_{c,i}$ is the critical current of the ith magnet, $\chi_i = \psi_i - \psi_{i-1}$ is the superconducting phase difference at this JJ, and $\varphi_{0,i}$ is the anomalous phase shift for a given JJ. In general, the anomalous phase shift $\varphi_{0,i}$ in S/F/S JJs depends on the direction of magnetization $\boldsymbol{m}_i$. The particular form of this dependence is determined by the type of spin-orbit coupling. For definiteness we consider Rashba-type SOC because it arises due to the structural inversion asymmetry and is the most common type of SOC for low-dimensional ferromagnets and thin-film ferromagnet/normal metal (F/N) hybrid structures. In this case the anomalous phase shift takes the form

$$\varphi_0 = r\hat{\boldsymbol{j}} \cdot (\boldsymbol{n} \times \boldsymbol{m}), \tag{1}$$

where $\hat{\boldsymbol{j}}$ is the unit vector along the Josephson current and $\boldsymbol{n}$ is the unit vector describing the direction of the structural asymmetry in the system. For the case under consideration it is along the z axis. r is a constant quantifying the strength of the coupling between the magnetic moment and the condensate. It depends on the material parameters of the ferromagnet, Rashba constant α, and length of the ferromagnetic interlayer

and has been calculated in the framework of different models [24,28]. Equation (1) is also valid for the S/F/S JJs on top of the 3D TI, for which it has been predicted that $r = 2hd/v_F$ [35,50], where d is the length of the interlayer and v_F is the Fermi velocity of the surface conduction electrons in 3D TIs. The results presented below depend only on the symmetry of Eq. (1) expressing how the anomalous phase shift depends on the direction of the magnetization $\boldsymbol{m}_i$; the dependence of the constant r on the junction parameters is irrelevant for our conclusions. If we choose to have the x axis along the Josephson current, then the symmetry of our system dictates that

$$\varphi_{0,i} = r_i m_{yi}. \tag{2}$$

This relation also survives in the dynamic situation $\boldsymbol{m}_i = \boldsymbol{m}_i(t)$ and has been used to calculate the magnetization dynamics in voltage-biased and current-biased JJs [48–50,52]. Now it is clear that our choice of the magnetic easy axis along the y direction maximizes the magnetoelectric coupling between the magnetic moment and the superconducting phase.

In the framework of our model we assume that the critical current $I_{c,i}$ does not depend on the direction of the magnetization $\boldsymbol{m}_i$. In fact, the behavior of the critical current depends crucially on the particular type of S/F/S JJ considered. For example, it can be independent of the magnetization direction, as reported for ferromagnets with SOC [24], or it can depend strongly on the x component of the magnetization, which is the case for the ferromagnetic interlayers on top of a 3D TI [35,50]. For the case of two coupled JJs the influence of the dependence $I_c(\boldsymbol{m})$ on the results was considered in Ref. [20]. It was found that taking into account this dependence does not change the results qualitatively and just modifies the boundaries of different regimes.

The energy of the system consists of Josephson energies of all junctions and easy-axis anisotropy energies of all magnets:

$$E = \sum_{i=1}^{N}\left[\frac{\hbar I_{c,i}}{2e}[1-\cos(\psi_i - \psi_{i-1} - \varphi_{0,i})] - \frac{K_i V_{F,i}}{2} m_{yi}^2\right], \tag{3}$$

where the first term is the Josephson energy and the second term is the magnetic anisotropy energy. K_i is the anisotropy constant of the ith magnet, and $V_{F,i}$ is its volume. ψ_i is a phase of the ith superconductor (see Fig. 1). The current conservation dictates

$$I_{c,i}\sin(\psi_i - \psi_{i-1} - \varphi_{0,i}) = I_{c,j}\sin(\psi_j - \psi_{j-1} - \varphi_{0,j}) \tag{4}$$

for arbitrary i and j.

In general, one should take into account the phase gradient due to the supercurrent flowing through the system. This leads to the fact that the phase ψ_i of the ith superconductor is not constant, $\psi_i(x) = \psi_{i,l} + \kappa_i(I_{\rm chain}/I_{c,i})(x/L)$, where $\psi_{i,l}$ is the superconducting phase at the left end of the ith superconductor, L is its length, and the second term accounts for the phase gradient due to the supercurrent $I_{\rm chain}$ flowing through the system. The coefficient κ_i quantifies the relation between the superconducting phase gradient and the supercurrent and can be estimated as $\kappa_i \sim eI_{c,i}L/\sigma_S \Delta S$, where Δ is the superconducting order parameter, σ_S is the normal state conductivity of the ith superconductor, and S is its cross section. To simplify the analysis we disregard the order parameter phase gradient. Its influence on the phase diagram of the coupled system was investigated in Ref. [20] for the case of two JJs, and it was found that it results in a renormalization of the parameter r and does not qualitatively influence the results. In addition, numerical values of κ_i were estimated for realistic systems, and it was concluded that the phase gradient can be safely neglected at least up to submillimeter lengths of the superconductors [20].

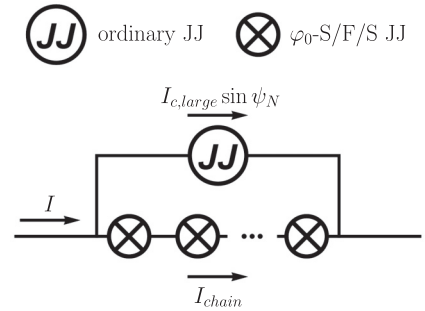

FIG. 2. Sketch of an asymmetric Josephson interferometer, where the coupled system of φ_0-JJs is parallel to an ordinary JJ with large critical current $I_{c,\rm large} \gg I_{c,i}$. The scheme allows us to control the phase ψ_N via the external current I (see text).

For the problem under consideration it is important to have a fixed phase difference ψ_N between the external superconducting leads and to have the possibility to control it. Experimentally, the phase ψ_N can be controlled in several ways. One of them is to insert the considered system into the superconducting loop under the applied magnetic flux. However, the direct proportionality between the Josephson phase and magnetic flux in a loop configuration holds only if the loop inductance is negligible. If it is non-negligible, peculiar effects may occur in the presence of φ_0-JJs [65], which requires additional care. The other way is to insert it into the asymmetric Josephson interferometer, where the considered system is parallel to an ordinary JJ with a much higher critical current. Then the magnetic state of the system can be controlled by the external current. In the present paper we consider the second method to control the external phase difference. A scheme of the corresponding system is presented in Fig. 2. The total external current I and the phase ψ_N between the external superconducting leads are related as

$$I = I_{c,\rm large}\sin\psi_N + I_{\rm chain}, \tag{5}$$

where $I_{c,\rm large}$ is the critical current of the additional ordinary JJ and $I_{\rm chain}$ is the current through the chain of φ_0-S/F/S JJs. We assume that $I_{c,\rm large} \gg I_{c,i}$. In this case $\psi_N \approx \arcsin[I/I_{c,\rm large}]$. All the calculations of the dynamics of our coupled φ_0-S/F/S JJs, which are discussed in Sec. IV, are performed for the system sketched in Fig. 2, where we set the external current I.

III. PHASE-CONTROLLED EQUILIBRIUM MAGNETIC STATE

First, we assume that all the coupled JJs are identical, that is, they all have the same parameters r, I_c, and KV_F. The influence of variations of these parameters is studied in

Sec. V. Then from Eq. (4) it follows that there are two possible solutions for the phase distribution along the chain of the coupled JJs. The first solution is that the total phase difference $\psi_i - \psi_{i-1} - \varphi_{0,i}$ at each of the JJs equals $\Phi + 2\pi n_i$, where n_i is an integer number. Φ can be found from the condition

$$\sum_{i=1}^{N}(\Phi + 2\pi n_i) = \sum_{i=1}^{N}(\psi_i - \psi_{i-1} - \varphi_{0,i}), \tag{6}$$

which gives

$$\Phi = \frac{\psi_N}{N} - \frac{\sum_{i=1}^{N}\varphi_{0,i}}{N} + \frac{2\pi n}{N}, \tag{7}$$

where $n = \sum_{i=1}^{N} n_i$ is an integer number. Substituting this solution for the phase distribution into the Josephson energy, we obtain the following expression for the total energy of the system:

$$E = NE_J(1 - \cos\Phi) - E_M \sum_{i=1}^{N} m_{yi}^2, \tag{8}$$

where $E_J = \hbar I_c/2e$ and $E_M = KV_F/2$.

The second solution of Eq. (4) is given by the total phase difference $\psi_i - \psi_{i-1} - \varphi_{0,i} = \pi - \Phi_u - 2\pi n_i$ at M JJs and $\psi_i - \psi_{i-1} - \varphi_{0,i} = \Phi_u + 2\pi n_i$ at the $N - M$ remaining JJs. In this case, analogously to the derivation of Eq. (7), we obtain

$$\Phi_u = \frac{\psi_N - \sum_{i=1}^{N}\varphi_{0,i} + 2\pi n - \pi M}{N - 2M}, \tag{9}$$

where $M < N/2$. The total energy of the system takes the form

$$E = E_J[N - (N - 2M)\cos\Phi_u] - E_M \sum_{i=1}^{N} m_{yi}^2. \tag{10}$$

For a given magnetic configuration, that is, for given values of m_{yi} at all weak links, the total energy of the system $E(\psi_N)$, described by Eq. (8), as a function of the phase difference between the external superconducting leads ψ_N has N different branches. The total energy described by Eq. (10) has $N - 2M$ branches for a given M. Our numerical analysis shows that all the energy branches described by Eq. (10) are unstable; that is, for a given ψ_N the system cannot live at such a branch and immediately goes to one of the branches described by Eq. (8).

Further, using Eq. (8), we can investigate which magnetic configurations of the system are stable in the system for a given set of parameters E_J, E_M, and r. Because the magnetic energy of the system is a concave function of m_{yi} and the Josephson energy depends on only the magnetizations in the combination $\sum_{i=1}^{N}\varphi_{0,i} = r\sum_{i=1}^{N} m_{yi}$, the minima of E as a function of $\{m_{yi}\}$ can be located only at the edges of the hypercube build on $\{m_{yi}\}$. That is, the minima can be only at points where no more than one $|m_{yi}| \neq 1$. Then we can find a minimum of the energy with respect to all m_{yi} independently.

Under the condition $\mathrm{sgn}[m_{yi}]\partial E/\partial m_{yi}|_{m_{yi}=\pm 1} < 0$ "corner states" $m_{yi} = \pm 1$ are minima of the energy. This condition is fulfilled irrespective of the external phase difference ψ_N if $2E_M/E_J > r$. This regime is not interesting if our goal is to control the magnetic configuration via the external phase. For this reason in our study we focus on the opposite regime,

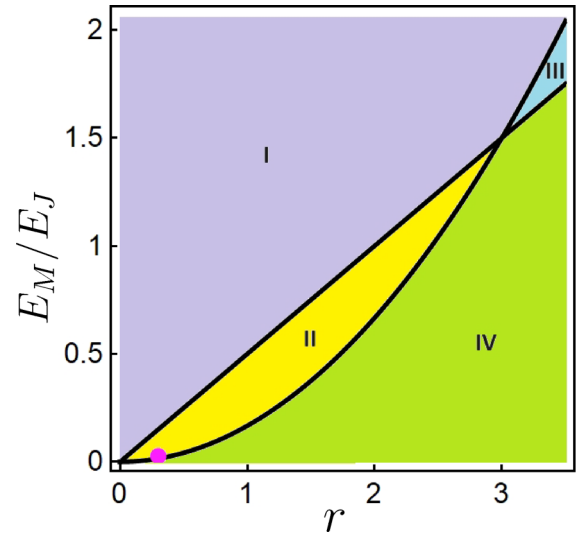

FIG. 3. Phase diagram of the coupled φ_0-S/F/S JJs. The lines $2E_M/E_J = r$ and $2E_M/E_J = r^2/N$ divide the diagram into regions I, II, III, and IV. For description of the regions see text. The pink point indicates parameters $(r, E_M/E_J)$ for which static and dynamic results presented in Figs. 4–8 are calculated.

$2E_M/E_J < r$, where there is a solution

$$\sin\Phi = 2E_M/rE_J \tag{11}$$

corresponding to the condition $\partial E/\partial m_{yi} = 0$, at which the magnetic configuration, corresponding to a given energy branch, becomes unstable. This parameter region allows us to control the magnetic configuration by adjusting the external phase.

There is also another important condition which determines the behavior of the magnetic configuration. One can define parameter regions where only magnetic configurations corresponding to corner states $m_{yi} = \pm 1$ are stable and parameters regions where $m_{yi} \neq \pm 1$ ("nonaligned states") are possible. To find the corresponding parameter regions we have to analyze when $|m_{yi}| \neq 1$ can be a minimum of the energy. For this purpose we consider the conditions $\partial E/\partial m_{yi} = -2E_M m_{yi} - E_J r\sin\Phi = 0$ and $\partial^2 E/\partial m_{yi}^2 = E_J r^2\cos\Phi/N - 2E_M > 0$. From these conditions we find that the most favorable conditions for the realization of a state $m_{yi} \neq \pm 1$ are at $\cos\Phi = 1$; that is, $\sin\Phi = 0$, and $m_{yi} = 0$. This situation can be realized if

$$\frac{2E_M}{E_J} < \frac{r^2}{N}. \tag{12}$$

The above considerations can be summarized in the form of a phase diagram, which is represented in Fig. 3. The lines $2E_M/E_J = r$ and $2E_M/E_J = r^2/N$ divide the diagram into four regions. In region I nonaligned states are not allowed, and all the corner states are always stable for an arbitrary Ψ_N. In region II nonaligned states are not allowed, but corner states can become unstable for some phase difference. In region III nonaligned states are allowed, and all corner states are stable for an arbitrary Ψ_N. In region IV nonaligned states are allowed, and all magnetic configurations become unstable for some value of Ψ_N. This phase diagram is a generalization of

the phase diagram discussed in Ref. [20] to the case of an arbitrary number of φ_0-S/F/S JJs with $N \geqslant 2$.

Parameters E_M/E_J and r were estimated in Ref. [20] for the model of the insulating ferromagnet on top of the 3D TI. If we take the parameters corresponding to $Nb/Bi_2Te_3/Nb$ Josephson junctions [66] (the junction length $d = 50$ nm, $I_c = 40$ A/m, and $v_F = 10^5$ m/s) and assume $K \sim [(10–10^2)\ \mathrm{erg/cm^3}] \times d_F$ for yttrium iron garnet (YIG) thin films [67], where $d_F = 10$ nm is the F thickness along the z direction, then we obtain $E_M/E_J \sim 10^{-2}$–10^{-1}. On the other hand, if, for a ferromagnetic weak link, we consider permalloy with very weak anisotropy, we can estimate $K \sim 10^3\ \mathrm{erg/cm^3} \times d_F$ [48]. This gives us $E_M/E_J > 1$. Therefore, different regimes from $E_M/E_J \ll 1$ to $E_M/E_J > 1$ can be realized experimentally. Based on the experimental data for the Curie temperature of the magnetized TI surface states [60], for which a Curie temperature in the range 20–150 K was reported, we can roughly estimate $h \lesssim 0.01 - 0.1 h_{\mathrm{YIG}}$ for YIG/3D TI interlayers. This corresponds to the dimensionless parameter $r = 2hd/v_F \lesssim 2 - 13$. On the other hand, r should be much smaller for ferromagnetic interlayers with intrinsic SOC and for combined interlayers consisting of a ferromagnet and a heavy metal because of the reducing factor $\Delta_{\mathrm{so}}/\varepsilon_F$ [24], which is typically considerably less than unity. Here Δ_{so} is a typical value of the SOC-induced splitting of the electron spectra, and ε_F is the Fermi energy of the material. From these estimates it follows that, in principle, all regions of the phase diagram could be experimentally accessible.

Further, we choose parameters of the system belonging to region II (the pink point in Fig. 3) and investigate the equilibrium and dynamic behavior of the system for the chosen set of parameters. This set of parameters is chosen because of (i) the possibility to control the magnetic configuration by the external phase, (ii) the smallness of typical realistic values of E_M/E_J [20] (except for ferromagnets with very weak magnetic anisotropy), and (iii) the absence of the nonaligned states, which complicate the physical picture. According to Eqs. (2), (7), and (8) the Josephson energy depends on only the total projection $M_y = \sum_{i=1}^{N} m_{yi}$ of all the magnets on the easy axis. For this reason in the absence of the nonaligned states there are only $N + 1$ essentially different magnetic configurations corresponding to $M_y = \{-N, -N + 2, \ldots, N - 2, N\}$. For each of the configurations $E(\psi_N)$ has N branches, which differ by a value of Φ, as described above and quantified by Eqs. (7) and (8).

In Fig. 4 we demonstrate low-energy branches of $E(\psi_N)$ for $N = 3$. There are four possible magnetic configurations, and for each of the configurations the lowest-energy branch is plotted. The other branches are not shown because they do not participate in the processes of dynamical switching between the magnetic configurations, described below. The dashed parts of the curves represent the parts of the corresponding branch where the magnetic configuration becomes unstable. The distance from the minimum of the corresponding branch, determined by the condition $\sin\Phi = 0$, to the point of instability, where the branch becomes dashed, according to Eq. (11) is determined as

$$\Delta\psi_N = N \arcsin\left[\frac{2E_M}{rE_J}\right]. \tag{13}$$

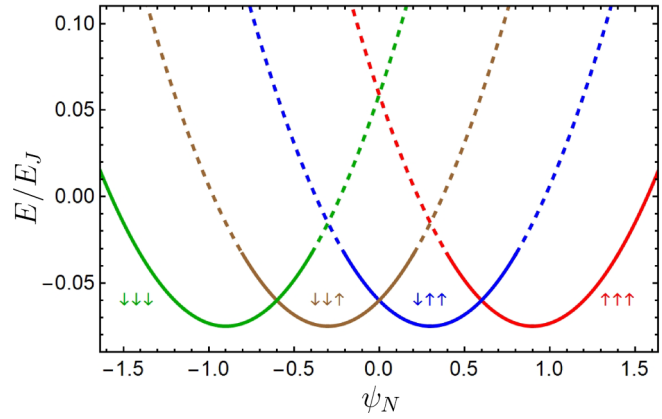

FIG. 4. Lowest-energy branches of $E(\psi_N)$ for $N = 3$. There are four possible magnetic configurations. They are shown by arrows, and for each of them the lowest-energy branch is plotted in the corresponding color. The dashed parts of the curves represent the parts of the corresponding branch where the magnetic configuration becomes unstable. $r = 0.3$, and $E_M/E_J = 0.025$.

Therefore, the analysis of the energy of the chain of coupled φ_0-S/F/S JJs indicates that the system behaves similarly to an atom where all magnetic configurations are degenerate at $r = 0$, but nonzero r removes the degeneracy. The split states are characterized by different projections of the total magnetization M_y of the macroscopic atom on the easy axis. But unlike an atom in a Zeeman field, the order in energy of these split states can be changed by varying the external superconducting phase ψ_N, as illustrated in Fig. 4.

IV. DYNAMICS AND SWITCHING OF THE MAGNETIC STATE

Here we discuss several dynamical effects in the system of coupled φ_0-S/F/S JJs which directly illustrate the analogy between the system and the macroscopic n-level system. The dynamics of the ith magnet is described by the Landau-Lifshitz-Gilbert equation [68–70]:

$$\frac{\partial \boldsymbol{m}_i}{\partial t} = -\gamma \boldsymbol{m}_i \times \boldsymbol{H}_{\mathrm{eff}} + \alpha \boldsymbol{m}_i \times \frac{\partial \boldsymbol{m}_i}{\partial t} - \frac{\gamma r I_{\mathrm{chain}}}{2eMdd_F}[\boldsymbol{m} \times \boldsymbol{e}_y], \tag{14}$$

where γ is the gyromagnetic ratio, $\boldsymbol{H}_{\mathrm{eff}} = (K/M)m_y\boldsymbol{e}_y$ is the local effective field in the ferromagnet induced by the easy-axis magnetic anisotropy, and α is the Gilbert damping constant. The last term in Eq. (14) describes the spin-orbit torque exerted on the magnet by the electric current I_{chain} [20,53,71–73]. The torque is averaged over the ferromagnet thickness d_F along the z direction. The total current flowing through each of the JJs consists of the supercurrent and the normal quasiparticle current contributions [51]:

$$I_{\mathrm{chain}} = I_c \sin(\psi_i - \psi_{i-1} - \varphi_{0,i}) + \frac{1}{2eR_N}(\dot{\psi}_i - \dot{\psi}_{i-1} - \dot{\varphi}_{0,i}), \tag{15}$$

where R_N is the normal state resistance of a separate φ_0-S/F/S JJ. The dynamics of all magnetizations $\boldsymbol{m}_i$ is calculated numerically from Eqs. (14), (15), and (5).

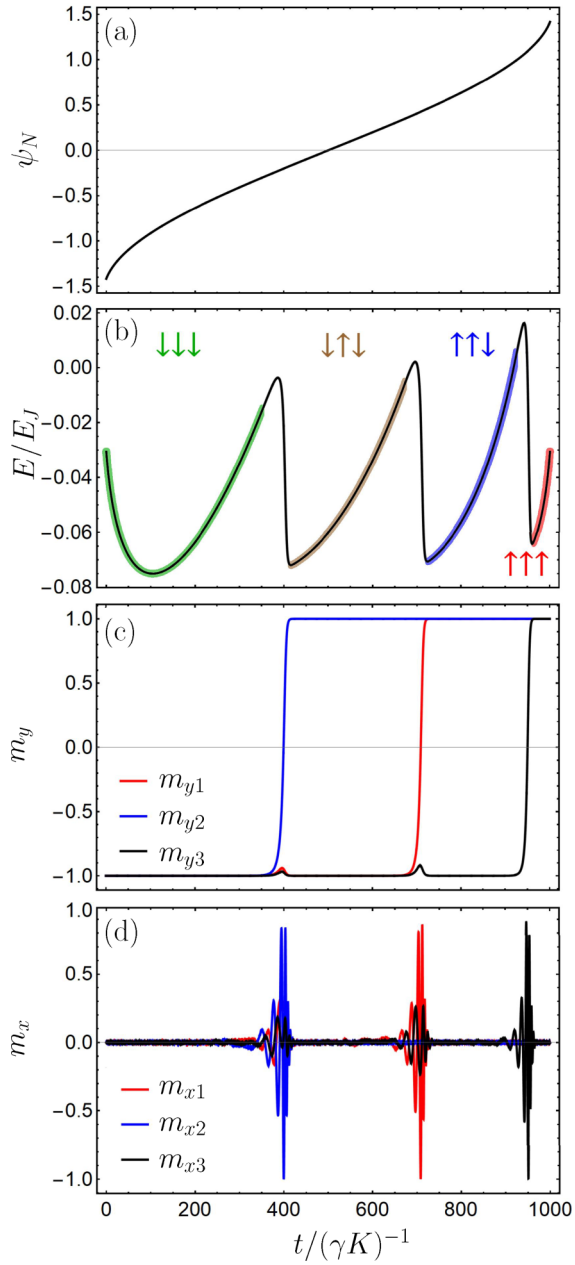

FIG. 5. Time evolution of the energy and magnetic configuration upon varying the external current from $-I_{c,\text{large}}$ to $I_{c,\text{large}}$ according to $I = (\beta t - 1)I_{c,\text{large}}$, with $\beta = 0.002(\gamma K)$. (a) External phase $\psi_N(t)$. (b) Energy of the coupled chain of φ_0-S/F/S JJs as a function of time. Intervals of t in which the system is in one of its stationary states are shown in colors corresponding to the states in Fig. 4. (c) $m_{yi}(t)$ and (d) $m_{xi}(t)$ for all magnets. $r = 0.3$, $\frac{E_M}{E_J} = 0.025$, $\alpha = 0.1$, and $I_{c,\text{large}}/I_c = 100$.

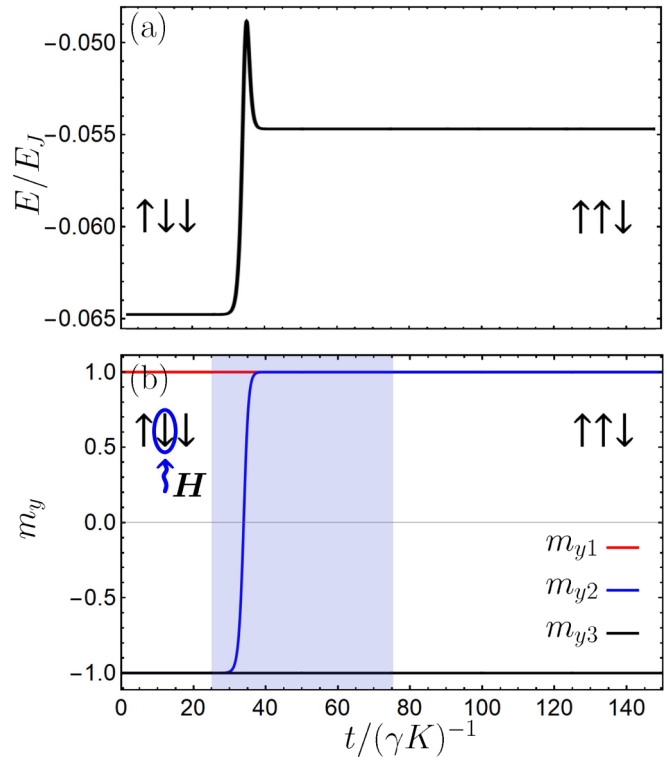

FIG. 6. Time evolution of (a) the system energy and (b) easy-axis projections of all magnets m_{yi} under external reversal of $\boldsymbol{m}_2$ by the pulse of an applied magnetic field. Magnetic field $\boldsymbol{H} = 4K\boldsymbol{e}_y$ is applied during the time interval shown by the shaded region in (b). $r = 0.3$, $\frac{E_M}{E_J} = 0.025$, $\alpha = 0.1$, and $\psi_N = -0.05$.

First of all, we demonstrate that in the setup sketched in Fig. 2 any magnetic configuration can be realized by varying the external current I. Thus, the magnetic configuration is fully controllable by electric means. The results are presented in Fig. 5. Figure 5(a) is auxiliary and demonstrates the dependence of the external phase difference on time when we vary the external current $I \propto t$. Figure 5(b) represents the dependence of the total energy of the system on time. In some ranges of t the system is in its stationary states, shown in Fig. 4. These time intervals are additionally shown in colors corresponding to the colors used in Fig. 4. Figures 5(c) and 5(d) illustrate the time evolution of all magnetic moments. $m_{yi}(t)$ are presented in Fig. 5(c), and $m_{xi}(t)$ are plotted in Fig. 5(d). $m_{zi}(t)$ are not shown because they behave very similarly to $m_{xi}(t)$.

Further, we study the dynamics of the system caused by an external reversal of one of the magnets. To reverse one of the magnets we fix a definite value of the external current I which corresponds to a particular stable magnetic configuration and apply a magnetic field $\boldsymbol{H} = \pm 4K\boldsymbol{e}_y$ during the time interval $\Delta t = 50(\gamma K)^{-1}$ to one of the magnets. The resulting dynamics can be very different. Since the physics of the magnetic system is not determined by a magnetic interaction with any characteristic spatial scale, the reversal of a given magnet can cause reversals of any magnet in the system. The dynamics is determined by only the order and stability of the energy levels of the system for a given phase.

In Fig. 6 we demonstrate that if the initial magnetic configuration is stable and, for a given phase difference, there is another stable state corresponding to a higher energy, it is possible to excite the system to this state. We reverse one of the magnets; the resulting state is stable, and the system remains in this state. In Fig. 6(a) we plot the dependence of the total energy of the system on time, and Fig. 6(b) represents the time evolution of all magnetic moments.

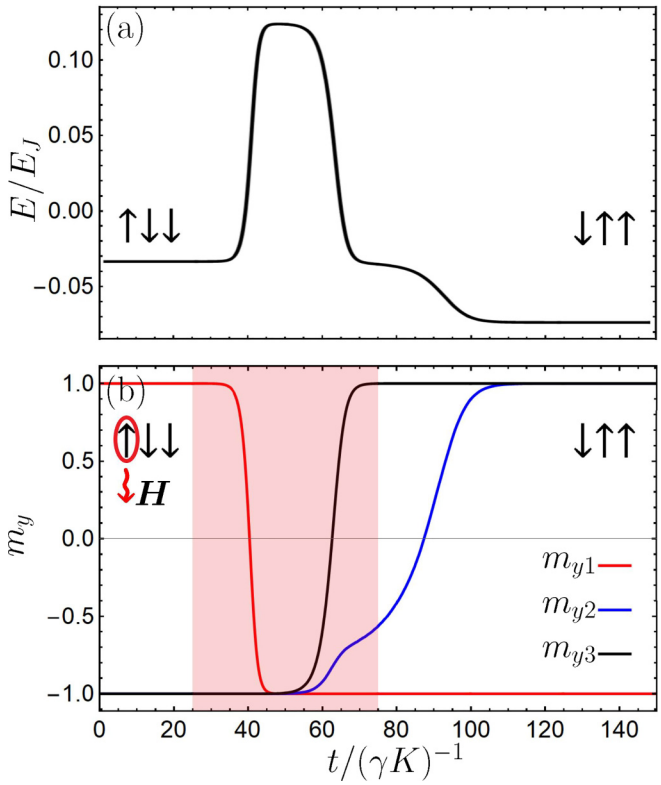

FIG. 7. The same as in Fig. 6, but for a different external phase difference ψ_N. Magnetic field $\boldsymbol{H} = -4K\boldsymbol{e}_y$ is applied to $\boldsymbol{m}_1$ during the time interval shown by the shaded region in (b). $r = 0.3$, $\frac{E_M}{E_J} = 0.025$, $\alpha = 0.1$, and $\psi_N = 0.20$.

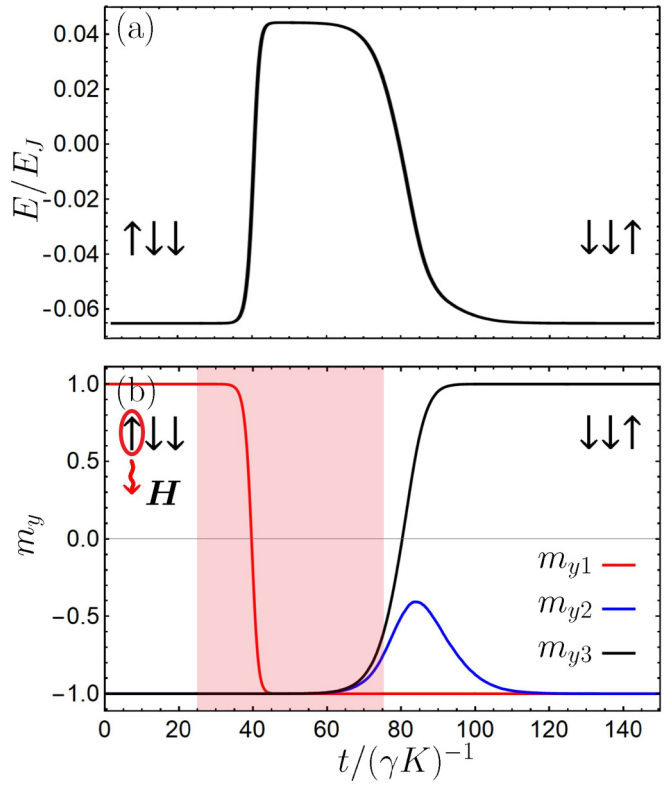

FIG. 8. The same as in Fig. 6, but for a different external phase difference ψ_N. Magnetic field $\boldsymbol{H} = -4K\boldsymbol{e}_y$ is applied to $\boldsymbol{m}_1$ during the time interval shown by the shaded region in (b). $r = 0.3$, $\frac{E_M}{E_J} = 0.025$, $\alpha = 0.1$, and $\psi_N = -0.05$.

In Figs. 7 and 8 we demonstrate the case in which the initial magnetic configuration is stable for the chosen phase difference but there is no stable state for the resulting magnetic configuration if we reverse one of the magnets. Then different possibilities can be realized. The first option is shown in Fig. 7. The reversal of $\boldsymbol{m}_1$ by the magnetic field pulse leads to the reversal of all the other magnets. As a result the system switches to the lower-energy state.

The other possibility is illustrated in Fig. 8. We reverse $\boldsymbol{m}_1$ using the external magnetic field. For the chosen phase difference there is no stable state for the resulting configuration ↓↓↓, and therefore, $\boldsymbol{m}_3$ is also reversed. But the probability that $\boldsymbol{m}_2$ is reversed is the same. In this case, a random magnet may be reversed; it is not determined by the distance from the externally reversed magnet.

Figures 6–8 demonstrate the results for $N = 3$ just as an example to illustrate the general behavior. If the chain consists of $N > 3$ φ_0-S/F/S JJs, then at a given ψ_N one can have more than two stable branches. An analogous increase of the number of stable branches (up to $N + 1$) can also occur if one changes the value of the parameter E_M/E_J without changing N. In this case by reversing one of the magnets we can reach any of these stable configurations at a given ψ_N. That is, the physics is the same as in Figs. 6–8, but there are more possible initial and final states of the system.

V. EFFECTS OF NONEQUIVALENCE OF JJs

Now we discuss how variations of the parameters K_i, $I_{c,i}$, and r_i describing individual φ_0-S/F/S JJs affect the results obtained above. We restrict ourselves to parameter regions I and II of the phase diagram, where nonaligned states do not occur. First of all, in this case variations of the magnetic anisotropy constant K_i do not influence $E(\psi_N)$. This is because at $m_{yi} = \pm 1$ the magnetic anisotropy energy depends on only the sum $\sum_{i=1}^{N} K_i$.

Now let us consider the influence of variations of the critical currents of individual JJs $I_{c,i}$. Small variations of the critical current do not influence $E(\psi_N)$. Indeed, we can write $I_{c,i} = I_{c,0}(1 + x_i)$, where $\sum_{i=1}^{N} x_i = 0$; that is, $I_{c,0}$ is the average critical current of all the JJs. We assume $x_i \ll 1$. Let us define an auxiliary parameter Φ_0 as $I_{\text{chain}} = I_{c,0} \sin \Phi_0$. Then $\Phi_i \equiv \psi_i - \psi_{i-1} - \varphi_{0,i}$ can be written as $\Phi_i \approx \Phi_0 + \delta\Phi_i$. From the condition $I_{\text{chain}} = I_{c,i} \sin \Phi_i = I_{c,0} \sin \Phi_0$ up to first order with respect to x_i we obtain $\delta\Phi_i \approx -x_i \tan \Phi_0$. Then $\sum_{i=1}^{N} \delta\Phi_i = 0$. From the conditions $\sum_{i=1}^{N} \delta\Phi_i = 0$ and $\sum_{i=1}^{N} x_i = 0$ it immediately follows that the first-order term in the expansion of $E(\psi_N)$ on x_i vanishes. Accounting for higher-order terms with respect to x_i can result in asymmetry and distortions of the energy branches.

The most essential effect on the physics of the N-level system, discussed in this work, can be caused by variations of r. They result in the additional splitting of the energy branches. If r is the same for all φ_0-S/F/S JJs, states $\{m_{y1}, m_{y2}, \dots\} =$

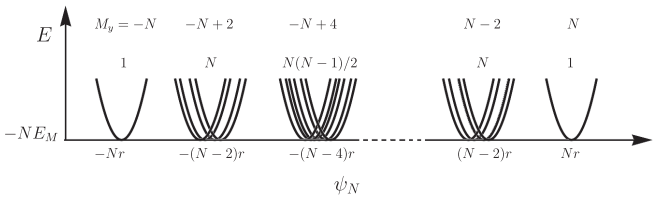

FIG. 9. Schematic illustration of the splitting of the lowest-energy branches, corresponding to different M_y. It is assumed that $\delta r_{ij} = |r_i - r_j| \ll \sum_{i=1}^{N} r_i/N$; otherwise, the splitting of each of the branches can become large, and curves originating from different initial configurations can be mixed. That does not modify the result qualitatively but makes it difficult to visually perceive the picture.

$\{+1, -1, \dots\}$ and $\{-1, +1, \dots\}$ are degenerate. However, if $r_1 \neq r_2$, according to Eq. (7), they have different values of Φ and therefore different energies. In general, if all r_i are different, an energy branch corresponding to $|M_y| = |N - 2K|$ is split over C_N^K branches. This is illustrated in Fig. 9, where the lowest-energy branches for each of the magnetic configurations are shown.

In addition at high enough temperatures close to the critical temperature and for JJs with small critical currents $I_{c,i}$ the system could also be sensitive to thermal fluctuations. The general stability of a single φ_0-JJ against thermal fluctuations has already been studied [52,74,75]. In our case of a chain of φ_0-JJs at a given ψ_N there are several stable states in the system. For this reason the thermal fluctuations will primarily spoil the stability of higher-energy metastable states. To minimize the destructive effect of thermal fluctuations, it is necessary to work at low temperatures and select larger JJs with large critical currents.

VI. CONCLUSIONS

In conclusion, we studied the static and dynamic magnetic properties of a system of N coupled φ_0-S/F/S Josephson junctions in which the anomalous ground state phase shift φ_0 provides direct coupling between magnetic moments and the phase of the superconducting condensate. The condensate phase, being a macroscopic quantity, mediates a long-range interaction between the magnetic moments. Due to this magnetoelectric coupling the system exhibits properties of an n-level system, where the corresponding energies are determined by only different projections of the total magnetic moment $\sum \boldsymbol{M}_i$ onto the easy axis, similar to a magnetic atom in a Zeeman field. However, unlike an atom in a magnetic field, the relative energies of different projections of the system's magnetic moment are controlled by the external phase difference. Further, we demonstrated that if one inserts the coupled chain of JJs into an asymmetric superconducting quantum interference device, one can reach any of the states corresponding to different projections of the total magnetic moment $\sum \boldsymbol{M}_i$ onto the easy axis by varying the external current. We also demonstrated that the long-range coupling between the weak links leads to highly nonlocal and nontrivial dynamics of the magnetic configuration under the application of a local external perturbation to one of the weak links. The dynamics is determined by only the order and stability of energy levels of the system for a given phase and therefore further supports the analogy to macroscopic n-level system.

ACKNOWLEDGMENTS

The analysis of the equilibrium properties of the system was supported by MIPT via Project No. FSMG-2023-0014. The studies of the dynamics were supported by RSF Project No. 22-42-04408.

[1] M. N. Baibich, J. M. Broto, A. Fert, F. Nguyen Van Dau, F. Petroff, P. Etienne, G. Creuzet, A. Friederich, and J. Chazelas, Phys. Rev. Lett. **61**, 2472 (1988).
[2] G. Binasch, P. Grünberg, F. Saurenbach, and W. Zinn, Phys. Rev. B **39**, 4828 (1989).
[3] P. Grünberg, R. Schreiber, Y. Pang, M. B. Brodsky, and H. Sowers, Phys. Rev. Lett. **57**, 2442 (1986).
[4] C. F. Majkrzak, J. W. Cable, J. Kwo, M. Hong, D. B. McWhan, Y. Yafet, J. V. Waszczak, and C. Vettier, Phys. Rev. Lett. **56**, 2700 (1986).
[5] M. B. Salamon, S. Sinha, J. J. Rhyne, J. E. Cunningham, R. W. Erwin, J. Borchers, and C. P. Flynn, Phys. Rev. Lett. **56**, 259 (1986).
[6] P. De Gennes, Phys. Lett. **23**, 10 (1966).
[7] L. R. Tagirov, Phys. Rev. Lett. **83**, 2058 (1999).
[8] D. N. Aristov, S. V. Maleyev, and A. G. Yashenkin, Z. Phys. B **102**, 467 (1997).
[9] P. V. Leksin, N. N. Garif'yanov, I. A. Garifullin, J. Schumann, V. Kataev, O. G. Schmidt, and B. Büchner, Phys. Rev. Lett. **106**, 067005 (2011).
[10] B. Li, N. Roschewsky, B. A. Assaf, M. Eich, M. Epstein-Martin, D. Heiman, M. Münzenberg, and J. S. Moodera, Phys. Rev. Lett. **110**, 097001 (2013).
[11] A. Di Bernardo, S. Komori, G. Livanas, G. Divitini, P. Gentile, M. Cuoco, and J. W. A. Robinson, Nat. Mater. **18**, 1194 (2019).
[12] A. Ghanbari, V. K. Risinggård, and J. Linder, Sci. Rep. **11**, 5028 (2021).
[13] Y. Zhu, A. Pal, M. G. Blamire, and Z. H. Barber, Nat. Mater. **16**, 195 (2017).
[14] A. E. Koshelev, Phys. Rev. B **100**, 224503 (2019).
[15] Z. Devizorova, S. V. Mironov, A. S. Mel'nikov, and A. Buzdin, Phys. Rev. B **99**, 104519 (2019).
[16] S. Mironov, A. S. Mel'nikov, and A. Buzdin, Appl. Phys. Lett. **113**, 022601 (2018).
[17] A. G. Mal'shukov, Phys. Rev. B **98**, 054504 (2018).
[18] Y. Lu, I. V. Tokatly, and F. S. Bergeret, arXiv:2307.10723.
[19] B. Xiang, Y. S. Lin, Q. He, J. Zhu, B. R. Chen, Y. F. Wang, K. Y. Liang, Z. J. Li, H. Yao, C. X. Wu, T. Zhou, M. Fang, Y. Lu, I. V. Tokatly, F. S. Bergeret, and Y.-H. Wang, Observation of long-range ferromagnetism via anomalous

supercurrents in a spin-orbit coupled superconductor (2023), https://api.semanticscholar.org/CorpusID:259991798.
[20] G. A. Bobkov, I. V. Bobkova, and A. M. Bobkov, Phys. Rev. B **105**, 024513 (2022).
[21] I. V. Krive, L. Y. Gorelik, R. I. Shekhter, and M. Jonson, Low Temp. Phys. **30**, 398 (2004).
[22] K. N. Nesterov, M. Houzet, and J. S. Meyer, Phys. Rev. B **93**, 174502 (2016).
[23] A. A. Reynoso, G. Usaj, C. A. Balseiro, D. Feinberg, and M. Avignon, Phys. Rev. Lett. **101**, 107001 (2008).
[24] A. Buzdin, Phys. Rev. Lett. **101**, 107005 (2008).
[25] A. Zazunov, R. Egger, T. Jonckheere, and T. Martin, Phys. Rev. Lett. **103**, 147004 (2009).
[26] A. Brunetti, A. Zazunov, A. Kundu, and R. Egger, Phys. Rev. B **88**, 144515 (2013).
[27] T. Yokoyama, M. Eto, and Y. V. Nazarov, Phys. Rev. B **89**, 195407 (2014).
[28] F. S. Bergeret and I. V. Tokatly, Europhys. Lett. **110**, 57005 (2015).
[29] G. Campagnano, P. Lucignano, D. Giuliano, and A. Tagliacozzo, J. Phys.: Condens. Matter **27**, 205301 (2015).
[30] F. Konschelle, I. V. Tokatly, and F. S. Bergeret, Phys. Rev. B **92**, 125443 (2015).
[31] D. Kuzmanovski, J. Linder, and A. Black-Schaffer, Phys. Rev. B **94**, 180505(R) (2016).
[32] A. G. Mal'shukov, S. Sadjina, and A. Brataas, Phys. Rev. B **81**, 060502(R) (2010).
[33] Y. Tanaka, T. Yokoyama, and N. Nagaosa, Phys. Rev. Lett. **103**, 107002 (2009).
[34] J. Linder, Y. Tanaka, T. Yokoyama, A. Sudbø, and N. Nagaosa, Phys. Rev. B **81**, 184525 (2010).
[35] A. Zyuzin, M. Alidoust, and D. Loss, Phys. Rev. B **93**, 214502 (2016).
[36] B. Lu, K. Yada, A. A. Golubov, and Y. Tanaka, Phys. Rev. B **92**, 100503(R) (2015).
[37] F. Dolcini, M. Houzet, and J. S. Meyer, Phys. Rev. B **92**, 035428 (2015).
[38] A. A. Burkov and D. G. Hawthorn, Phys. Rev. Lett. **105**, 066802 (2010).
[39] D. Culcer, E. H. Hwang, T. D. Stanescu, and S. Das Sarma, Phys. Rev. B **82**, 155457 (2010).
[40] O. V. Yazyev, J. E. Moore, and S. G. Louie, Phys. Rev. Lett. **105**, 266806 (2010).
[41] C. H. Li, O. M. J. van 't Erve, J. T. Robinson, Y. Liu, L. Li, and B. T. Jonker, Nat. Nanotechnol. **9**, 218 (2014).
[42] I. V. Bobkova, A. M. Bobkov, and M. A. Silaev, J. Phys.: Condens. Matter **34**, 353001 (2022).
[43] Y. M. Shukrinov, Phys. Usp. **65**, 317 (2022).
[44] W. Mayer, M. C. Dartiailh, J. Yuan, K. S. Wickramasinghe, E. Rossi, and J. Shabani, Nat. Commun. **11**, 212 (2020).
[45] D. B. Szombati, S. Nadj-Perge, D. Car, S. R. Plissard, E. P. A. M. Bakkers, and L. P. Kouwenhoven, Nat. Phys. **12**, 568 (2016).
[46] A. Assouline, C. Feuillet-Palma, N. Bergeal, T. Zhang, A. Mottaghizadeh, A. Zimmers, E. Lhuillier, M. Eddrie, P. Atkinson, M. Aprili, and H. Aubin, Nat. Commun. **10**, 126 (2019).
[47] A. Murani, A. Kasumov, S. Sengupta, Y. A. Kasumov, V. T. Volkov, I. I. Khodos, F. Brisset, R. Delagrange, A. Chepelianskii, R. Deblock, H. Bouchiat, and S. Guéron, Nat. Commun. **8**, 15941 (2017).
[48] F. Konschelle and A. Buzdin, Phys. Rev. Lett. **102**, 017001 (2009).
[49] Y. M. Shukrinov, I. R. Rahmonov, K. Sengupta, and A. Buzdin, Appl. Phys. Lett. **110**, 182407 (2017).
[50] M. Nashaat, I. V. Bobkova, A. M. Bobkov, Y. M. Shukrinov, I. R. Rahmonov, and K. Sengupta, Phys. Rev. B **100**, 054506 (2019).
[51] D. S. Rabinovich, I. V. Bobkova, A. M. Bobkov, and M. A. Silaev, Phys. Rev. Lett. **123**, 207001 (2019).
[52] C. Guarcello and F. S. Bergeret, Phys. Rev. Appl. **13**, 034012 (2020).
[53] I. V. Bobkova, A. M. Bobkov, I. R. Rahmonov, A. A. Mazanik, K. Sengupta, and Y. M. Shukrinov, Phys. Rev. B **102**, 134505 (2020).
[54] C.-Z. Chang, J. Zhang, M. Liu, Z. Zhang, X. Feng, K. Li, L.-L. Wang, X. Chen, X. Dai, Z. Fang, X.-L. Qi, S.-C. Zhang, Y. Wang, K. He, X.-C. Ma, and Q.-K. Xue, Adv. Mater. **25**, 1065 (2013).
[55] X. Kou, M. Lang, Y. Fan, Y. Jiang, T. Nie, J. Zhang, W. Jiang, Y. Wang, Y. Yao, L. He, and K. L. Wang, ACS Nano **7**, 9205 (2013).
[56] X. Kou, L. He, M. Lang, Y. Fan, K. Wong, Y. Jiang, T. Nie, W. Jiang, P. Upadhyaya, Z. Xing, Y. Wang, F. Xiu, R. N. Schwartz, and K. L. Wang, Nano Lett. **13**, 4587 (2013).
[57] C.-Z. Chang, W. Zhao, D. Y. Kim, H. Zhang, B. A. Assaf, D. Heiman, S.-C. Zhang, C. Liu, M. H. W. Chan, and J. S. Moodera, Nat. Mater. **14**, 473 (2015).
[58] Z. Jiang, F. Katmis, C. Tang, P. Wei, J. S. Moodera, and J. Shi, Appl. Phys. Lett. **104**, 222409 (2014).
[59] P. Wei, F. Katmis, B. A. Assaf, H. Steinberg, P. Jarillo-Herrero, D. Heiman, and J. S. Moodera, Phys. Rev. Lett. **110**, 186807 (2013).
[60] Z. Jiang, C.-Z. Chang, C. Tang, P. Wei, J. S. Moodera, and J. Shi, Nano Lett. **15**, 5835 (2015).
[61] Z. Jiang, C.-Z. Chang, C. Tang, J.-G. Zheng, J. S. Moodera, and J. Shi, AIP Adv. **6**, 055809 (2016).
[62] M. Gibertini, M. Koperski, A. F. Morpurgo, and K. S. Novoselov, Nat. Nanotechnol. **14**, 408 (2019).
[63] L. Ai, E. Zhang, J. Yang, X. Xie, Y. Yang, Z. Jia, Y. Zhang, S. Liu, Z. Li, P. Leng, X. Cao, X. Sun, T. Zhang, X. Kou, Z. Han, F. Xiu, and S. Dong, Nat. Commun. **12**, 6580 (2021).
[64] K. Kang, H. Berger, K. Watanabe, T. Taniguchi, L. Forró, J. Shan, and K. F. Mak, Nano Lett. **22**, 5510 (2022).
[65] C. Guarcello, R. Citro, O. Durante, F. S. Bergeret, A. Iorio, C. Sanz-Fernández, E. Strambini, F. Giazotto, and A. Braggio, Phys. Rev. Res. **2**, 023165 (2020).
[66] M. Veldhorst, M. Snelder, M. Hoek, T. Gang, V. K. Guduru, X. L. Wang, U. Zeitler, W. G. van der Wiel, A. A. Golubov, H. Hilgenkamp, and A. Brinkman, Nat. Mater. **11**, 417 (2012).
[67] J. Mendil, M. Trassin, Q. Bu, J. Schaab, M. Baumgartner, C. Murer, P. T. Dao, J. Vijayakumar, D. Bracher, C. Bouillet, C. A. F. Vaz, M. Fiebig, and P. Gambardella, Phys. Rev. Mater. **3**, 034403 (2019).
[68] L. D. Landau and E. M. Lifshitz, Phys. Z. Sowjetunion **8**, 153 (1935).
[69] T. L. Gilbert, IEEE Trans. Magn. **40**, 3443 (2004).

[70] M. Lakshmanan, Philos. Trans. R. Soc. A **369**, 1280 (2011).
[71] T. Yokoyama, Phys. Rev. B **84**, 113407 (2011).
[72] I. Mihai Miron, G. Gaudin, S. Auffret, B. Rodmacq, A. Schuhl, S. Pizzini, J. Vogel, and P. Gambardella, Nat. Mater. **9**, 230 (2010).
[73] I. V. Bobkova, A. M. Bobkov, and M. A. Silaev, Phys. Rev. B **98**, 014521 (2018).
[74] C. Guarcello and F. S. Bergeret, Chaos, Solitons Fractals **142**, 110384 (2021).
[75] C. Guarcello, F. S. Bergeret, and R. Citro, Appl. Phys. Lett. **123**, 152602 (2023).